Optical properties of Si-Ge-C nanostructures deposited by MBE

Detlev Grützmacher, Rainer Hartmann, Oliver Leifeld, Ulf Gennser, Christian David, Elisabeth Müller,

Jan-Christoph Panitz

Micro- and Nanostructures Laboratory, Paul-Scherrer-Institut, CH-5232 Villigen-PSI, Switzerland

ABSTRACT

Molecular beam epitaxy (MBE) has been used to deposit quantum structures in the material system Si-Ge-C in order to evaluate the possibilities for Si based opto-electronics. In particular the growth of Si/SiGeC quantum wells, the growth of quantum structures on pre-patterned Si substrates and the self-organised growth of Ge and C-induced Ge dots have been investigated. Studying the photoluminescence (PL) response of strained SiGeC quantum wells of various compositions and well widths by MBE the band discontinuities for compressively strained and lattice matched SiGeC/Si heterostructures have been determined. The data indicate a type I bandalignment in Si/SiGeC quantum well structures. By modifying the morphology, the chemistry or the strain of Si surfaces the formation of Ge quantum dots can be triggered. The growth of strained SiGe alloys on a small mesa leads to plastic relaxation of the strained film. The degree of relaxation depends on the thickness, the size, and the crystallographic orientation of the mesa. Phonon resolved PL spectra were obtained from the type II transition between the strained Si and the relaxed SiGe grown on small mesa structures. In addition, the self organised growth of Ge dots on bare and on C covered Si (100) surfaces has been studied. The deposition of 2-4 monolayers of Ge on these surfaces leads to the formation of small, irregularly shaped islands without facets. Intense photoluminescence is observed from samples containing multiple C-induced Ge island layers.

Keywords: Silicon molecular beam epitaxy, Ge quantum dots, band offsets, pre-patterned substrates

1. INTRODUCTION

Because of the technological background in Si processing there is great interest in expanding its capabilities, with the long term goal of combining optical and electronical components on single Si substrates. The design of new artificial structures within the system Si-Ge-C promises to furnish Si based systems with high speed and integrated optoelectronical functions. The first observations of band edge photoluminescence on fully strained $Si_{1-x}Ge_x$ alloys /1/ and $Si/Si_{1-x}Ge_x$ MQWs /2/ at the beginning of the 90's were a matter of great excitement. Compared to pure Si the luminescence efficiency could be increased by several orders of magnitude, an effect due to the localization of the charge carriers in the fluctuations of the alloy compositon and in the potential wells of MQWs. However, the efficiency is still low compared to that of direct band gap materials. In addition, the 2-dimensional growth of SiGe systems is limited by the built-in strain.

For a further improvement of the luminescence efficiency two major concepts have been followed: the transition of the indirect band structure to a direct band gap and the enhancements of charge carrier localization in quantum dots. Already in 1974 Gnutzmann and Clausecker /3/ showed that Brillouin Zone folding in short period Si_mGe_n superlattices (SLs) /4/ may result in a quasi-direct band gap.

Fundamental changes of the indirect band structure are also predicted for zero dimensional Si systems /5/. Decreasing the crystallite size below 5 nm is expected to open symmetry allowed transitions across the band gap. The emission of visible light from porous Si is observed up to room temperature /6/. The physical origin, whether Quantum Size Effect /6/ or other chemical or defect related mechanisms /7-10/, is still a matter of controversy /11,12/.

A better access to the luminescent mechanisms involved is given by self-organized nanostructures /13-16/. The in-situ growth avoids surface damage and improves the control over the crystallite size and density. Under certain conditions, an increase in the luminescence efficiency of SiGe dots compared to smooth SiGe layers was observed /17/. However, the fabrication of dots with uniform diameter of less than 50 nm remains a critical issue /18/. The substitutional incorporation of C /19/ is expected to lift the stress induced limitations of SiGe heteroepitaxy and to widen the design flexibility of group IV materials. The small covalent radius of C allows the growth of strain compensated SiGeC layers /19/ and strain symmetrized SiGe/SiC heterostructures /20/ of almost infinite critical thickness. Band gap and band alignment of C containing MQWs are still rather unclear. Recent results on Si/SiC MQWs indicate an efficient electron confinement within the SiC layers /21/.

This modified alignment of the conduction band promises new possibilities in the design of n-channel devices as well as optically active structures within materials of the group IV.

2. EXPERIMENTAL

The deposition of the Si-Ge-C structures discussed in this paper was performed by a MBE system (Balzers UMS 500). The deposition rate was adjusted to 1 Å/s for the Si and SiGeC layers. The Ge dots were fabricated using deposition rates of 0.1 Å/s for the Ge. The Si and Ge flux was controlled by mass spectroscopy /22/. The C was evaporated from a hot pyrolitic C filament. The evaporation rate was calibrated using secondary ion mass spectroscopy (SIMS).The substrates were generally wet chemically cleaned followed by an in-situ bake at 950°C in the MBE chamber for 30 min. After this treatment no decoration of the layer to substrate interface was detected by TEM.

For the wafer patterning the wafers were thermally oxidized and then coated with 15nm Cr and 50nm PMMA resist. Arrays of mesa lines and mesa squares were generated by low voltage electron beam lithography over an area of several square millimeters. The PMMA resist pattern was transferred into the Cr layer by reactive ion etching in a Cl_2/CO_2 plasma. The remaining Cr served as a highly selective mask for a reactive ion etching step in a $CHF_3/SF_6/O_2$ plasma deep into the Si substrate. The 15nm thick SiO_2 layer underneath the Cr cover protected the mesa top from damage during the RIE step and was removed by a HF lift-off to give a clean, defect free, and passivated Si surface.

The PL is excited at 2.2 K by the $\lambda = 488$ nm line of an Ar^+ laser and detected by a nitrogen-cooled Ge photodetector. The Raman spectra were measured with a Labram II Raman confocal microscope. The internal He-Ne laser ($\lambda = 632$ nm) and an external Kr ion laser ($\lambda = 530.9$ nm) were used for excitation of Raman spectra in the 200-1200 cm^{-1} range. The pinhole diameter was adjusted to 200 µm, corresponding to a lateral resolution of 2 µm. Voigt profiles with fixed Gaussian linewidths corresponding to the spectral resolution of 3 cm^{-1} were fitted to the experimentally obtained data in order to calculate band positions and linewidths.

3. RESULTS AND DISCUSSION

3.1 Bandoffsets in Si/SiGeC Quantum Well Structures

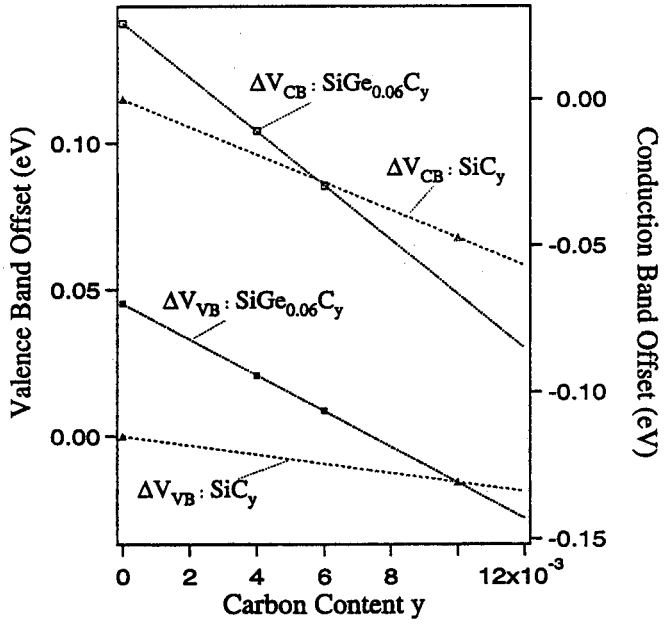

Fig.1: Band offsets for unstrained $Si_{1-y}C_y$ and $SiGe_{0.06}C_y$ (Fig.4)as a function of y . The offsets are given relative to the Si band edges.

The bandoffset in compressively strained SiGe quantum wells embedded in Si occurs mainly in the valence band /2/, and it was just recently that intensive studies of the photoluminescence (PL) signal explored over a wide range of excitation densities showed that the bandalignment is of type II, i.e. the conduction band forms a shallow barrier for electrons at the SiGe layer /23/. At high excitation densities band bending leads to a type one behavior of the SiGe well. On the other side, tensilely strained SiC alloys embedded in Si form a type I quantum well with about 70% of the banddiscontinuity in the conduction band. The band offsets for SiGeC quantum wells embedded in Si are still under debate /8,24/ and depend certainly on the composition of the alloyed layer.

Within certain limitations PL measurements can be used to extract the band alignments. In our excitation dependent PL measurements we did not observe band bending, therefore it is not considered in the calculation. However, the excitation power might have been too large to obtain the effect. Furthermore, any interface smearing due to Ge, C and Si interdiffusion is neglected and a constant binding energy of 15 meV is assumed. In addition, carrier localization is not taken into account. Using this approximation a simple Kronig-Penney model is used to deduce the band offsets from PL measurements of multiple quantum wells (MQW) with

constant compositions but different layer widths. For the calculation the effective Δ(4) electron mass of Si bulk material $m_{\Delta(4)} = 0.19\ m_0$ and the effective heavy hole mass of SiGe is used for the SiGeC quantum well taking the strain related band splitting into account. For the barrier the effective mass of the transverse Δ(2) Si electron state $m_{(\Delta 2)} = 0.92\ m_0$ is used. A detailed study for slightly compressive strained as well as lattice matched SiGeC quantum wells is published elsewhere /25/. Here we try to get a more comprehensive analysis of the band offsets covering the whole range of Ge concentrations between 0 and 15% and C concentrations between 0 and 1.5% by interpolating between the experimental data /25/ and extrapolating from those values.

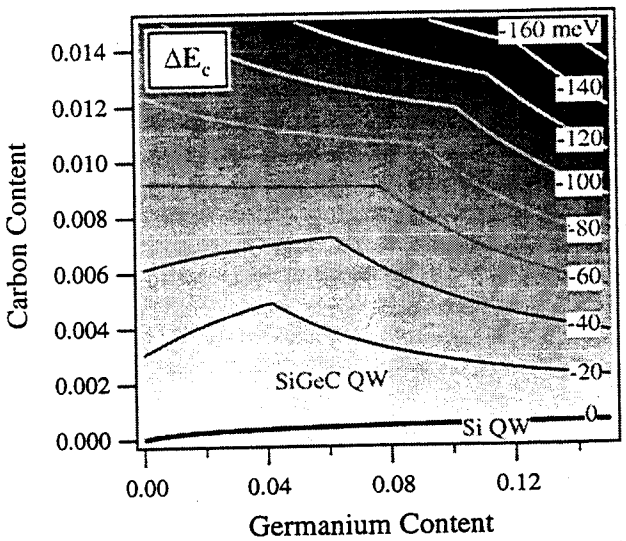

Fig.2: Energy of the $Si_{1-x-y}Ge_xC_y$ conduction band edge relative to the Si band edge as a function of Ge and C concentration

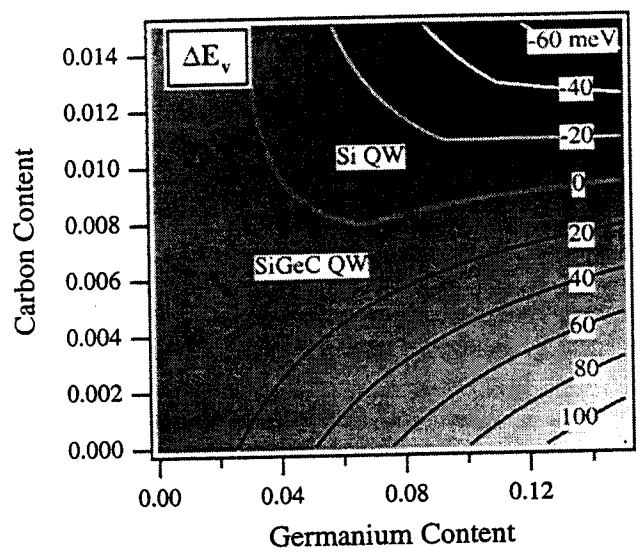

Fig.3: Energy of the $Si_{1-x-y}Ge_xC_y$ valence band edge relative to the Si band edge as a function of Ge and C concentration.

Fig. 1 shows the bandoffsets for unstrained $Si_{1-y}C_y$ and $Si_{0.94-y}Ge_{0.06}C_y$ as a function of the Carbon content y. The amount of the offsets due to strain is calculated by model solid theory and subtracted from the experimental data, the remaining data are fitted using the Kronig-Penney model leading to the band offsets for unstrained structures. Fig. 1 indicates that the band between unstrained Si and SiC_y, respectively $SiGe_{0.06}C_y$ linearly depend on the C content. We now make the additional assumption, that they also have a linear dependence on the Ge content. It is then possible to interpolate linearly between the two lines for $Si_{1-y}C_y$ and $SiGe_{0.06}C_y$ in fig. 1, for the alloys with $0<x<0.06$ and $0<y<0.008$. Through a linear extrapolation, this is extended to the experimentally relevant region $0<x<0.15$ and $0<y<0.015$. Although this linear approximation seems reasonable for a certain range of Ge and C content, it is clear that the scant experimental data warrants future investigations. Encouraging sign for the validity of the map thus drawn out is the linearity of the band gap dependence on C and Ge content, respectively. In addition, the extrapolation of the band offsets has proven to be able to describe the experimental luminescence energies of pseudomorphic, 45Å wide $SiGe_{0.06}C_y$ MQWs of different y and $SiGe_xC_{0.004}$ MQWs of different x /25/. In fig.2 (conduction band) and fig.3 (valence band) the offsets are presented, when the strain effects are re-incorporated. The band offsets are shown as contour lines illustrating the layer compositions with constant band discontinuities. The kinks in the equi-offset lines in fig.2 correspond to the strain compensated alloys, where the Δ(2) and Δ(4) conduction bands are degenerated. To the left or right of these kinks the alloys are either tensilely or compressively strained, with the band minima constituted by the Δ(2) or Δ(4) band, respectively.

Let us first consider how the offsets move with the Ge concentration, for a constant C content, starting from the position of the strain compensated kink. For a reduction in x, there will be an increase in the tensile strain, pulling down the Δ(2) conduction band and lifting up the lh valence band. Simultaneously, the unstrained, degenerated SiGeC conduction band moves up with respect to the Si band for [C]<0.6%, and decreases for [C]>0.6% (moving vertically in fig. 1). Thus, for [C]<0.6%, where the strain and intrinsic effects push the offset in the same

direction, a reduction of the Ge concentration in strain compensated SiGeC increases the conduction band offset. With increasing C concentration (0%<[C]<0.6%) the intrinsic impact on the band energy decreases and completely vanishes for [C]=0.6%. In this case the strain alone determines the variation of the conduction band offset of the Si - tensilely strained $Si_{1-x-y}Ge_xC_y$ junction. For higher C content, the intrinsic and strain induced effects will start to cancel each other, until, for [C]>0.9% the intrinsic shifts are dominating, and the conduction band offset decreases with decreasing Ge content x . In the valence band (Fig.3), the intrinsic and stress induced effects are balancing each other out, except for quite high Ge concentrations, and for most alloys with tensile strain the valence band offset is not very large.

If we now instead increase the Ge content, the compressive strain will shift down the Δ(4) conduction band and lift up the hh valence band with respect to the Si band edge. Intrinsic conduction band offset and strain effects are moving in the same direction for [C]>0.6%. Thus, the conduction band offset strongly increases with the Ge content x. For [C]<0.6% the addition of Ge shifts the unstrained conduction band edge to higher energy and, thus, reduces the strain induced energy decrease of the Δ(4) state. This is seen fig.2. The slope of the contour lines in the compressive strain region decreases with decreasing C content in SiGeC. Whereas for the tensile region a compensation between the intrinsic and strain induced effects is reached for [C]=0.9%, this balance is not achieved for compressive strain until y ~0. This is of course the well known 'zero' conduction band offset for Si/SiGe junctions. The valence band offset in the compressive region is almost solely determined by the intrinsic band offsets, the uniaxial strain and hydrostatic pressure shifts of the hh band acting in opposit directions. It is observed, that for sufficiently high C content, the valence band offset shows a confinement in the Si layer instead of the SiGeC layer. This can already be surmised from the fits of the PL from pseudomorphic $Si/SiGe_{0.06}C_y$ MQWs (y=0.004 and y=0.006), where a decreasing valence band offset was found for increasing C content. Whether and where this leads to an inversion of the Si and SiGeC valence band alignment depends on the details of the extrapolation, and needs to be investigated in further experiments.

The variation in the conduction band alignment (Fig.2) may seem surprising: SiGe is known to have a very small conduction band offset, and when increasing the Ge content in the $Si_{1-x-y}Ge_xC_y$ alloy one would think that the offsets would be closer to that of the $Si_{1-x}Ge_x$ alloy. However, as we have seen, the addition of C suppresses the balance between the intrinsic offset and the strain effects. This demonstrates that care has to be taken to separate different effects, when using the simple picture of ternary SiGeC as an intermediate between SiGe and SiC

As we stated above, figs.2 and 3 have to be taken with grain of salt, due to the extrapolation made. However, they indicate the possibility of obtaining respectably large conduction band offsets, either in tensilely strained SiC quantum wells with sufficiently high C content or in compressively strained Si/SiGeC structures. Until further measurements, the values of the conduction band offsets are still speculative, but as long as the offsets retain a linear dependence on the Ge and C concentration, our analysis indicates that if the offset in an alloy with higher Ge content is smaller than given here, then the offset in the SiC alloy is instead larger than estimated, and vice versa.

To conclude, through linear extrapolation we calculated the values of the band discontinuities in $Si/Si_{1-x-y}Ge_xC_y$ MQWs within the composition region 0%<x<15% and 0%<y<1.5%. It is demonstrated that ternary SiGeC cannot simply be considered as an intermediate between SiGe and SiC. Our map of the band offsets indicates that both electron and hole confinement in SiGeC are possible without the need of relaxed buffer layers. This, together with the diffusion quenching effects of C makes the SiGeC alloy a potential candidate for CMOS technology as well as for optical devices. In particular the type I alignment over a wide range of compositions makes the Si-Ge-C system potentially interesting for the preparation of quantum boxes confined in Si.

3.2. Growth on Prepatterned Si (100) Substrates

In this approach to reduce the dimensionality from 2-D to 1- or 0-D structures, two concepts are used. Growing on prestructured surfaces exposing surfaces with different crystallographic orientation may lead to the formation of quantum wires and quantum dots due to the differences in growth rate between adjacent surface facets /26/. In addition the growth on small pedestals may lead to a change in the relaxation mechanism when strained material is deposited on them /27/. It can be expected that the size and orientation of such small mesa structures has an impact on the relaxation and consequently on the band gap of the grown layer. Therefore structuring of Si surfaces prior to growth appears an potential tool for the formation of nanostructures in the material system Si-Ge-C. To study the impact of size and orientation of mesa structures on the relaxation mechanism of SiGe, lines of different widths and crystallographic orientation were etched into Si (100) surfaces by reactive ion etching (RIE). Subsequently the structure was overgrown by a SiGe graded buffer layer followed by a 300 nm thick $Si_{0.76}Ge_{0.24}$ layer and a SiGe/Si MQW structure, forming a type II bandalignment which provides a quantum well in the Si for the electrons and a confinement for the holes in the SiGe layers. Mesa lines of 2 mm length and a width ranging from 2-10 μm were prepared. The orientation of the mesa lines was varied from lines along the [110] direction to those along the

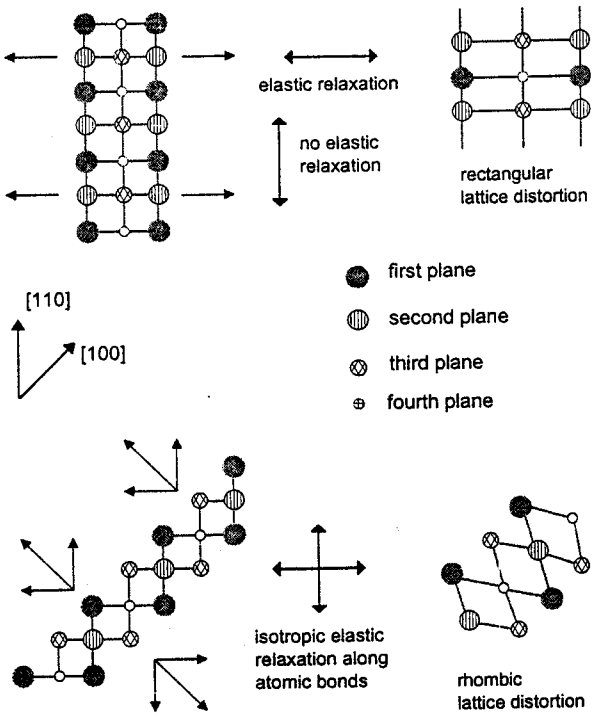

Fig. 4: Illustration of the elastic deformation of a diamond crystal lattice on top of [110] (upper) and [100] (lower) oriented mesa lines. Anisotropic and isotropic deformation behavior can be tailored by the mesa orientation.

Second on the [110] oriented mesas only dislocations perpendicular to the mesa line are obtained, no dislocations along the mesa line are detected, whereas the dislocation pattern on the [100] oriented mesas is symmetric. This indicates that the mesas along the [110] direction contain an uniaxial strain component. The strong reduction in the dislocation density can also be observed by TEM. Fig. 6 shows a cross sectional view of a structure with 1.5 μm wide mesa lines separated by 1 μm wide grooves. The lines were oriented along the [100] direction. No dislocations are obtained in the SiGe buffer layer grown on top of the mesa, whereas the material grown in the grooves exhibits many dislocations. The dislocation network is particularly dense at the Si sidewalls etched by the RIE process. Damage caused by the RIE process apparently acts as nucleation centers for the dislocations. In addition quite a few dislocations cross the Si pedestals or "jump" through the substrate from one groove filled with SiGe to the adjacent one. These dislocations cause the Si pedestals to deform and partly adopting the SiGe lattice parameters. We therefor propose that not only elastic deformation of the pedestals may cause the SiGe to relax but also this new kind of dislocations in the Si pedestals. The sidewalls of the SiGe layer exhibit {064} and {046} facets and only a narrow {100} facet on top. The inset of fig.6 shows a close-up of the Si/SiGe quantum well structure grown in the topmost layer. The smaller growth rate on the side facets is clearly visible by the smaller periodicity of the MQW structure.

[100] direction in steps of 15°. Besides the geometry and size of the growth zone, the crystallographic orientation of line shaped mesas is expected to influence the strain relaxation. Plastic relaxation occurs through the propagation of misfit dislocations along the [111] planes, and thus may be affected by the orientation of the mesa stripes. The orientation dependent variations of the elastic strain relief are illustrated in fig.4. For mesa lines along [110] the elastic lattice deformation only extends the atomic bonds perpendicular to the zone edge, while the bonds parallel to the mesa stripe are unaffected. This anisotropy becomes lifted for the [100] oriented ridges, where all bonds close to the edge of the growth zone can expand elastically, thus leading to a rhombic lattice distortion.

Fig. 5 shows surface scans from a atomic force microscope (AFM) from samples containing mesa lines along the [100] and [110] direction. The width of the mesa lines was 4 μm for the AFM measurements; due to the faceted growth on top of the mesa AFM could not be performed on narrower lines. First of all clearly less dislocation are obtained on top of the mesa ridges than on the non-patterned areas.

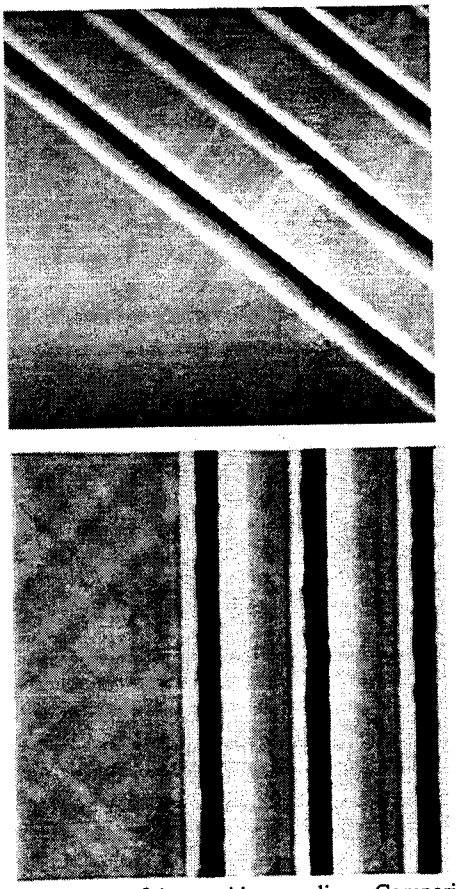

Fig.5: AFM scans of 4 μm wide mesa lines. Comparison of cross-hatch pattern on mesa lines and unpatterned surfaces. Top: lines along [110]; bottom: lines along [100]

However, from this measurements no conclusive answer can be given to the question how much strain is left in the material grown on top of the mesa ridges. For this purpose micro-Raman spectroscopy was performed. Scanning across the mesa lines and monitoring the peak position of the Si-Si vibrations on top and in between the mesa lines may permit to compare the strain state on the different surface textures. But due to the faceted growth the Ge composition on top of the mesa may change as well, making the situation rather complex. In general the Si-Si vibration is found at smaller wavenumbers on top of the mesa than within the grooves, indicating either a higher degree of relaxation or a higher Ge concentration on top of the mesa. The difference of roughly one wavenumber accounts for a difference of 1.5% in the Ge content or for a change in the degree of relaxation of 20% between the top of the mesa and the bottom of the grooves. Since this difference is found also between the center region of wide mesa structures, where faceting is less important, and the grooves, a change in the degree of relaxation appears to be more likely. Apparently the material in the 0.7 μm wide grooves is still compressively strained despite the large number of dislocations seen in the cross-sectional TEM. No noticeable difference in the position of the Si-Si vibration line has been found between Raman spectra taken from unpatterned areas of the wafer and from the top of mesa lines running along the [100] directions, independently from the widths of the mesa. For lines along the [110] direction a shift of 0.5 cm^{-1} towards higher wavenumbers is obtained when the width of the mesa line is reduced from 4μm to 2μm. Since faceting and consequently any effect on the Ge content is less pronounced for lines along the [110] directions compared to lines along the [100] directions, we assign this shift again to a difference in the degree of relaxation. Wide lines are relaxed via dislocations, whereas the relaxation of narrow lines is obviously incomplete. As indicated by the AFM these lines contain only a few dislocation perpendicular to the line shaped mesa and elastically they are only able to deform into a rectangular distortion of the lattice (see Fig. 4), therefore we think that these lines contain some uniaxial strain.

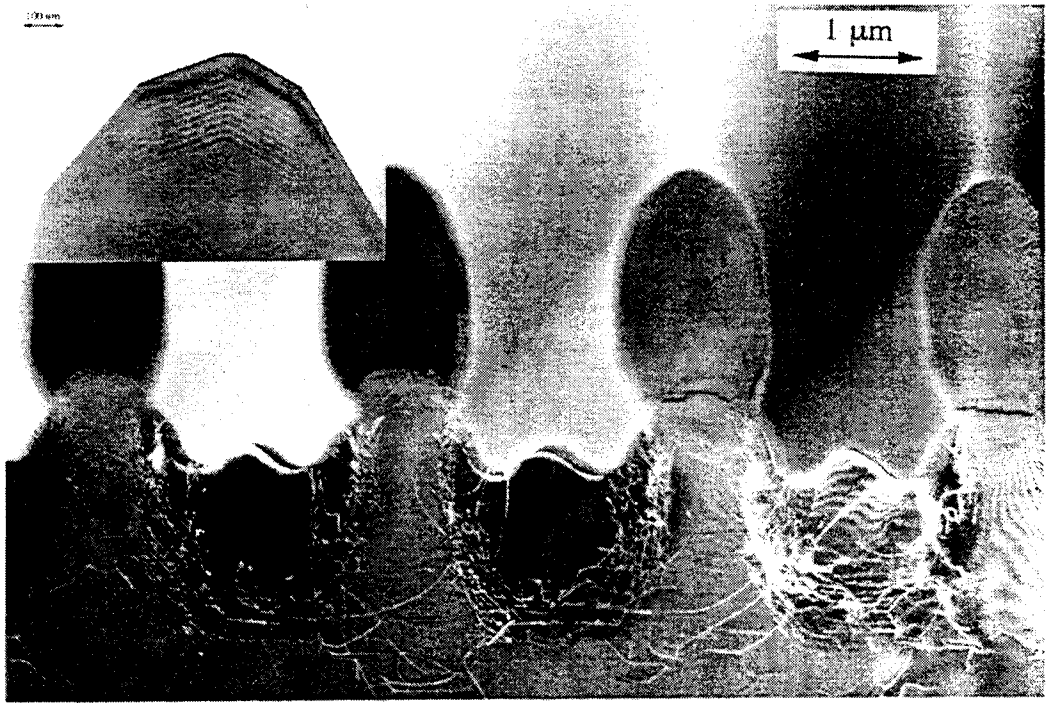

Fig.6: Cross-sectional TEM of a step graded Sige buffer layer with a Si/Sige MQW structure on top grown on 1.5 μm wide mesa lines oriented along the [100] direction. Inset: Topmost Si/SiGe MQW with 1.5 nm wide Si quantum wells

Comparing Raman spectra of narrow mesa lines along the [110] and 15° off the [110] direction with those along the [100] and up to 15° off the [100] direction, the latter ones show a more pronouced shift of the Si-Si vibration between the spectra taken from the top of the mesa and the bottom of the grooves, indicating that the SiGe grown on the mesa lines along the [100] direction are either to an higher degree relaxed or contain more Ge. Following the argumentation above, we think that the relaxation is improved for SiGe grown on the lines in the [100] direction.

Fig.7 depicts PL spectra taken from areas with mesa lines oriented along a) the [110] direction and b) 15° off the [100] direction. Each graph shows the dependence of PL spectra on the widhts of the mesa lines, in addition fig. 7b also shows a reference spectrum of an unpatterned region from the same sample. The PL of the unpatterned region as well as those from

broad mesa lines is dominated by a broad signal at 750-950 meV, which is attributed to the dislocation network. The luminescence of the $Si_{0.76}Ge_{0.24}$ layer is very weak (marked by B^{TO} and B^{NP} in fig.7). This luminescence of the SiGe layer is shifted monotonously towards smaller energies with decreasing widths of the mesa lines from 10 to 2 μm in Fig.7a, i.e. for lines along the [110] direction, whereas no shift is obtained for the $Si_{0.76}Ge_{0.24}$ luminescence in fig.7b, i.e. grown on the lines oriented 15° off the [100] direction. The situation for 3 and 2.5 μm wide mesa lines is somewhat unclear.

In both cases the broad band PL related to the dislocation network decreases strongly in intensity for narrow mesa linewidths and the PL of the SiGe gains in intensity. However, comparing the spectra taken from the structure grown on the narrowest mesa lines a distinct difference in the energetic position of the most prominent PL doublet is identified. In fig.7a the doublet with peak positions at 1011 and 956 meV is assigned to the no-phonon (NP) and TO phonon transition of the thick $Si_{0.76}Ge_{0.24}$ layer, respectively, whereas the doublet in fig. 7b at 970 and 914 meV is interpreted as no-phonon transition and TO phonon replica of the type II transition of the Si/SiGe MQW structure. The energetic position appears to be correct for a transition of electrons confined in 1.6 nm wide Si wells and holes confined in the 20 nm wide SiGe layers. This interpretation is further supported by the observation that the doublet in fig. 7b vanishes after etching off the topmost Si/SiGe MQW structure and only weak PL of the $Si_{0.76}Ge_{0.24}$ buffer layer remains. The absence of quantum well related PL in fig.7a can be explained by the less complete relaxation of the SiGe, leaving some strain in the SiGe and also reducing the tensile strain in the Si layers and thus reducing the conduction band discontinuity, i.e. the confinement potential for electrons in the Si wells.

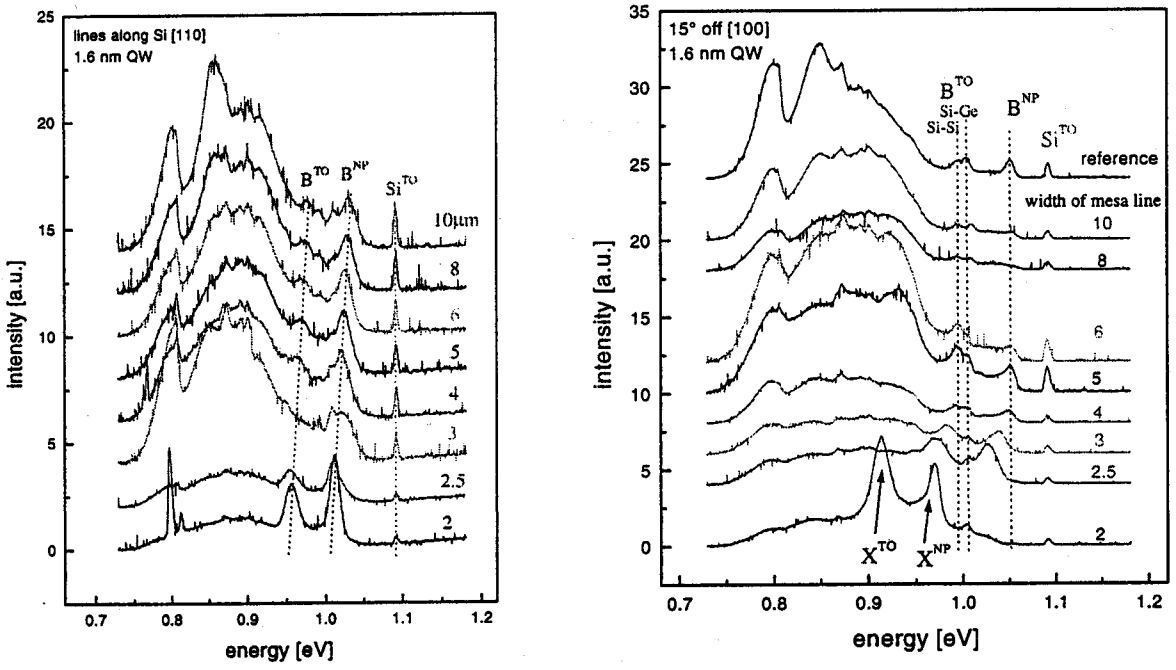

Fig.7: PL spectra of a Si/SiGe MQW on top of a step graded $Si_{0.76}Ge_{0.24}$ buffer layer grown on mesa lines oriented a) along the [110] and b) 15° off the [100] direction.

Even though the mechanism of strain relaxation on these line shaped mesa is not completely understood and in particular the amount of strain left in the SiGe buffer layers is not exactly known the occurance of the strong quantum well related PL indicates that the concept of varying the size and orientation of mesa lines opens new possibilities in the design of optically active heterostructures in the Si-SiGe material system.

3.3 C-Induced Ge Quantum Dots

Lateral carrier confinement by the self assembled growth of quantum dots has been proven a powerful method to fabricate low dimensional structures /13-15/. During growth the built-in stress can be relieved without the introduction of lattice defects by the spontaneous formation of hut clusters /16/. The diameter of the clusters depends on the growth temperature and low temperatures (< 500°C) are necessary to reduce the diameter below 50 nm. However, the lack in material quality at low temperatures quenches any Ge dot luminescence /28/. Recently it has been demonstrated that Ge islands as small as 10

nm in diameter and 1 nm in height can be produced at moderate growth temperatures on Si (001) surfaces coated with a sub-monolayer of carbon. Intense PL with pronounced NP emission has been reported and interpreted as a spatially indirect recombination between electrons confined in a C-rich wetting layer and holes confined in the Ge rich region of the dot /29/. Recently we studied the effect of sub-monolayer C coatings on the Si surface reconstruction in detail /30/. STM investigations show islands exhibiting a C-induced c(4x4) reconstruction of the Si (001) surface as well as an increase in surface roughness after the C deposition. TEM micrographs reveal a pronounced dot formation for the deposition of 2.5 ML of Ge on Si (100) surfaces covered with 0.1-0.3 ML of C /31/. These dots forming at Ge coverages below the critical thickness of Ge on Si have an irregular shape and exhibit no facets /31/. In this paper we present a detailed analysis of the PL data from Ge dots formed by 2.5 - 4 ML of Ge on these C-coated surfaces.

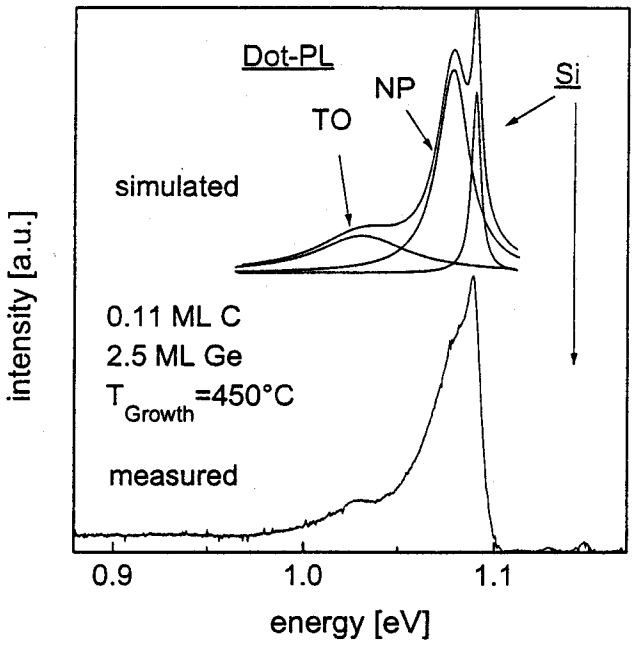

Fig. 8: Typical PL spectrum of Ge dots induced by the pre-deposition of C and completely embedded into Si. 0.11 ML C and 2.5 ML Ge are deposited at T_{Growth}=450°C . The PL spectrum is taken without post-growth RTA of the sample and with an laser excitation intensity of $P_{unfocused}$=11mW .

A typical PL spectrum taken on a sample with 0.11 ML predeposited C and a Ge overlayer thickness of 2.5 ML, grown at 450°C, is shown in fig.8. A strong NP PL line at 1.09 eV, close to the Si TO peak, and its TO replica at 1.04 eV are observed. A careful separation of the NP and Si TO line gives a rather large linewidth of about 20 meV for the NP line.

The NP signal and the transverse optical phonon replica are identified as excitonic recombination in the C induced Ge dots. The strong PL intensity without post-growth annealing may result from a spatially indirect recombination process /29/. The electrons are confined in an underlying C rich $Si_{1-x-y}Ge_xC_y$ wetting layer, the hh in the Ge rich upper part of the Ge islands. Because of the gradual composition variation, the electron and hole wavefunctions deeply penetrate into the neighboring dot region and strongly overlap each other. The linewidth of 20 meV is attributed to a broad dot size distribution. In contrast to conventionally grown Ge dots /28/ separate wetting layer luminescence is not observed. This may support the model of a spatially indirect charge recombination, or may be due to the small average dot spacing of less than the diffusion length of the excited charge carriers.

The energy position of the luminescence does not only depend on the size of the Ge dots but also on the amount of C deposited. Smaller amounts of C reduce the offset in the conduction band, thus increasing the recombination energy. The linewidths may depend on the growth temperatures. Slightly higher growth temperatures are likely to increase the size homogeneity and to decrease the linewidth (Fig. 9).

We are aware that the assignment of the two PL lines at 1.03eV and 1.08eV as quantum dot luminescence and not wetting layer luminescence is not completely unambiguous. However, there are several indications supporting our interpretation, and they are the subject of the following discussion.

The enhanced appearance of the NP PL line of fig. 8 may be explained by the lateral confinement of the charge carriers in the quantum dots. In-plane exciton localization due to interface roughness has recently been found to lead to enhanced NP luminescence /32/. Three-dimensional confinement relieves otherwise strict momentum conservation required for dipole allowed recombination across the indirect band gap, and phononless PL due to k-diagonal recombination are obtained /33/.

The dependence of PL spectra on the deposition temperature (T_{Growth}=350°C - 750°C) of the self-assembled growth of C induced Ge dots is summarized in fig. 9. At the substrate temperature of 350°C the sample exhibits the deep, broad band signal, which is typical for MBE growth at low temperatures. The defect related luminescence band is suppressed for T_{Growth}=450°C, and dot luminescence can be observed. Increasing the temperature to 550°C the BB signal completely vanishes, and the quantum dot PL remains visible. At T_{Growth}=650°C and T_{Growth}=750°C the dot luminescence is quenched, and only Si related signals appear in the spectra. At these high temperatures C is known to locally accumulate on the surface and to form silicon carbide precipitates /34, 35/. In fact lattice defects and imperfections have been found by careful TEM

analysis of these samples. The PL spectra are in good agreement with the TEM studies where clear islanding is observed for T_{Growth}=450°C and T_{Growth}=550°C.

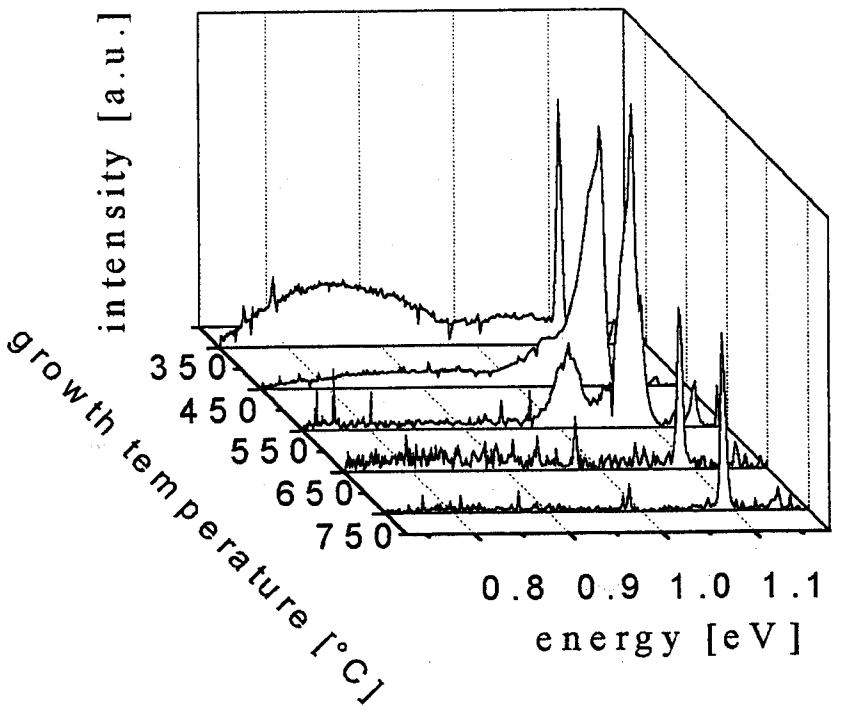

Fig.9: Dot luminescence for different growth temperatures. For T_{Growth}=350°C the spectra are dominated by broad band luminescence.Only Si related signals are detected for T_{Growth}=650°C and T_{Growth}=750°C , respectively. Dot luminescence occurs for T_{Growth}=450°C and T_{Growth}=550°C.

Comparing the 450°C and 550°C sample, the dot related signal linewidth is reduced, and the TO/NP intensity ratio is increased for the latter. In addition, the PL is shifted by few meV to higher energies. For the higher growth temperature a more homogeneous dot size distribution can be expected. The enhanced surface diffusion may coalesce the Ge adatoms into larger quantum dots at the expense of the smaller ones. Thus, the difference in the luminescence energies originating from the different Ge dots shrinks, leading to an overall reduction of the signal linewidth. The increase of the TO/NP intensity ratio may indicate a partial transition to a more quantum well like double peak feature of the PL spectra at higher growth temperatures. The PL red-shift for T_{Growth}=550°C may be related to a reduced confinement of the electrons in the C rich wetting layer and the holes in the Ge rich dot area due to interdiffusion. Annealing studies on C induced Ge dots /36/ are assumed to have a similar impact on the PL spectra as the increase of the growth temperature. Diffusion processes smear out the interfaces between the dots and the surrounding Si and, thus, change the characteristic shape of the dot luminescence. Fig. 10 shows a series of PL spectra measured on samples before and after a 4 min RTA at temperatures varying between 550°C and 1100°C. For the anneal temperatures of 550°C and 650°C the dot related luminescence slightly shifts to higher energies by ~ 8 meV and increases in intensity by a factor of about 3. In addition, the TO replica becomes resolved. The gain in the PL intensity compared to the as grown sample is attributed to the healing of the point defects which reduces the number of non-radiating recombination centers. For anneal temperatures between 750°C and 1050°C the energy shift and the decrease of the intensity ratio between NP and TO phonon are enhanced. The luminescence signals remain visible even for anneal temperatures of at least 1050°C, i.e. for anneal temperatures which are much higher than the growth temperature of quenching PL signals (Fig. 9). The 950°C RTA shifts the NP peak by 38meV, and the signal from the TO replica becomes stronger in intensity than the NP line. For T_{Anneal}=1100°C only the substrate related PL signals are resolved. The energy shift and the change of the intensity ratio can be explained by a diffusion process. Intermixing Ge and Si causes the dots to smear out. Thus, the Ge concentration within the dots decreases, and the wider distribution of Ge reduces the carrier confinement. This causes an energy blueshift. At the same time, thickness fluctuations become less important reducing the linewidth of the PL peaks. Finally, the Ge islands develop a flat Si/SiGeC structure with a gradual concentration profile, and this becomes obvious in the more quantum well like double peak feature of the PL spectra. The pronounced energy blueshift and the evolution from one broad photoluminescence peak to two well resolved lines reflect a gradual transition from quantum dot states to quantum well-like states /36/. Due to the limited number of density of states in zero dimensions dot luminescence is expected to shift to higher energies when the exciting laser intensity is increased. For low excitation intensities only the Ge dots with largest lateral sizes, and thus with lowest confinement shifts become populated with charge carriers. An increasing laser intensity subsequently populates the smaller quantum dots with energy states of higher energies, thus increasing the high energy contributions to the PL signal. Such a blueshift with an energy saturation at rather low excitation intensities is observed in the PL spectra of fig.11, where the intensity of the unfocused laser beam is

varied between 0.01mW and 11mW . The saturation behavior is also observed in the intensities of the dot PL relative to the substrate related signals. For increasing excitation power the intensity ratio between dot luminescence and Si TO signal decreases.

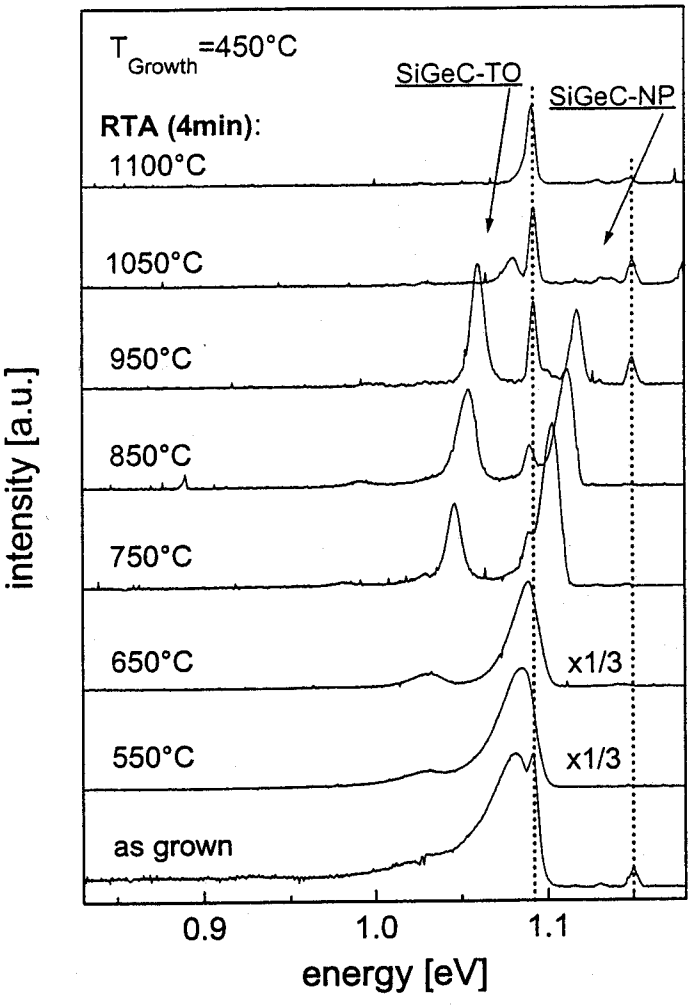

Fig.10: Series of 2.2K -PL spectra taken on the sample with 0.11ML of predeposited C and 2.5ML of Ge, grown at T_{Growth}=450°C , before and after a 4min RTA at temperatures between 550°C and 1100°C. The excitation intensity is $P_{unfocused}$=2.75mW. An energy blueshift and an evolution from one broad PL peak to two well resolved lines are observed with increasing RTA temperature. The dotted lines in the spectra give the positions of the Si PL.

The linewidth of the dot line is expected to increase with increasing excitation power since a large number of dots with different sizes are contributing to the signal. A quantitative fitting of the PL spectra is difficult due to the low energy separation between the dot and substrate related PL. However, a linewidth broadening does not seem to occur. We want to point out that PL blueshift of about the same order also occurs when the luminescence changes from BE recombination at low power intensities to FE recombination at high power intensities /2/. Furthermore, saturation behavior at low excitation intensities is also found for impurity luminescence. On the other hand, excitation dependent PL measurements on the C induced Ge dot samples do not exhibit any shift of the luminescence signals (Fig. 12) after they have been annealed at 950°C . The constant energy may be related to the more homogenous size distribution and the higher density of states in the SiGeC quantum wells compared to the Ge dots. The different impact of the laser excitation on the PL spectra before and after the thermal treatment of the samples, therefore, seems to be related to changes of the carrier confinements and may support the assignment of quantum dot PL for the as grown sample.

Further evidence for the dot luminescence can be found from the PL spectra from samples with different average Ge cluster sizes. TEM and STM studies show that the Ge dots grow in size when the Ge coverage increases from 2.5ML to 4ML at a constant Si coating with 0.11ML C. The PL spectra of the samples with 2.5, 3 and 4 monolayers of Ge (Fig. 13) reveal strong dot related emission for the smallest dots with 2.5ML Ge, that weakens and red-shifts with increasing amount of Ge coverage. The linewidth increases with Ge overlayer thickness, and already for 3ML Ge NP and TO signal do not appear well resolved.

The PL redshift with increasing Ge deposition can only be explained by assuming dot luminescence. Dots increasing in size shift the quantum confined sub-bands to lower energies, thus decreasing the energy gap between the $\Delta(2)$ and hh states. Luminescence signals from the underlying $Si_{1-x-y}Ge_xC_y$ wetting layer would not be expected to shift to higher energies. Before the onset of the island formation the addition of Ge gradually compensates the tensile strain of the $Si_{1-y}C_y$ layer. Strain compensation widens the band gap leading to a PL blueshift in this case /29/. In the regime of island formation - and that is the present regime according to TEM and STM studies /31/ - the additional deposition of Ge does not change the composition and thickness of the wetting layer, and no PL shift is expected. A signal redshift with increasing Ge concentration does not occur for the PL from the wetting layer both for the two- and three-dimensional growth regime. The observed broadening of the linewidth results from an increasingly in-homogenous dot size distribution. PL redshift and increasing PL linewidth are correlated with three-dimensional growth. The intensity loss for 4ML Ge may be related to an increasing strain in the dot layer and the onset of faceted island formation /31/.

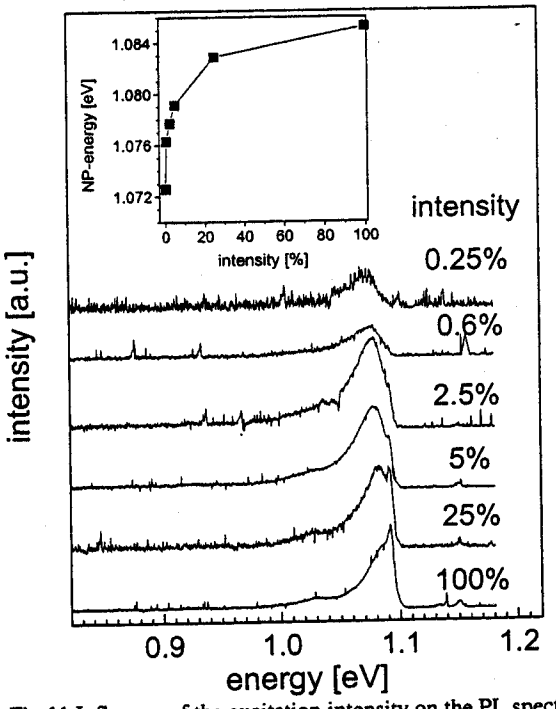

Fig.11 Influence of the excitation intensity on the PL spectra of C induced Ge dots. The intensity is given in percentage of the incoming Ar^+ -laser light $P_{unfocused}$=11mW. The sample contains 0.11ML of predeposited C and 2.5ML of Ge, grown at 450°C . The energy shift is plotted in the inset.

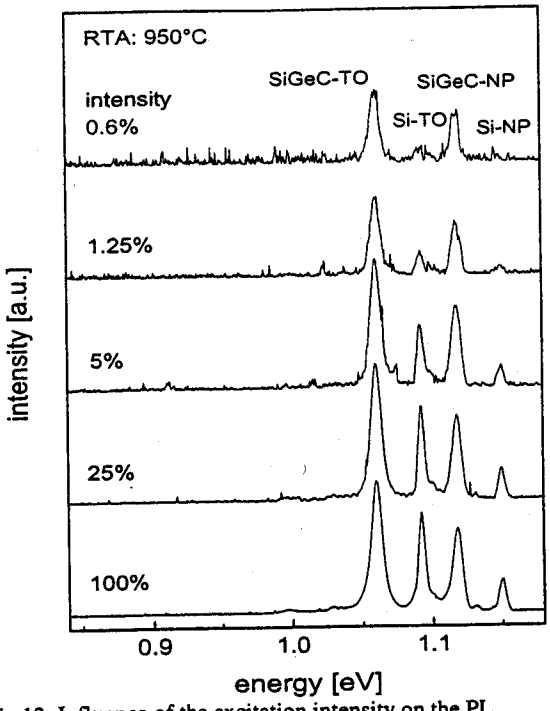

Fig.12: Influence of the excitation intensity on the PL spectra of the C induced Ge dot sample of fig.11 after it has been annealed at 950°C for 4min. The intensity is given in percentage of the incoming Ar^+ laser light ($P_{unfocused}$=11mW)

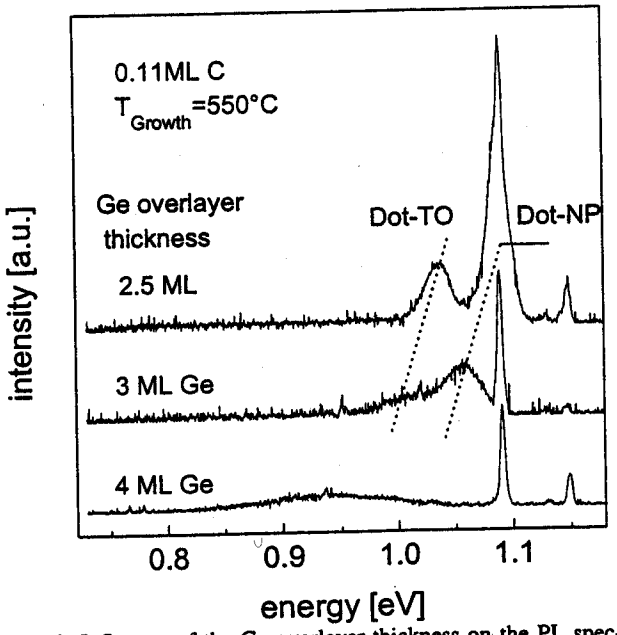

Fig. 13: Influence of the Ge overlayer thickness on the PL spectrum of C induced Ge dots. Strong dot related emission is observed from the smallest dots with 2.5ML Ge, which weakens and red-shifts with increasing Ge coverage. (T_D= 550°C)

In conclusion, luminescence is observed from the C induced Ge dot structures, and the signals are believed to originate from the Ge islands. Our interpretation is supported by the suppression of the phonon replica in the PL spectra. The changes of the photoluminescence with substrate temperature is shown to be correlated with the dot formation as observed by TEM. The enhancement of the TO line with increasing growth and anneal temperature, respectively, reflects the gradual transition from zero- to two-dimensional charge recombination. This is supported by the influence of the excitation intensity on the PL spectra, which is different for the samples before and after the RTA processing. Finally, we varied the Ge coverage, and the redshift and broadening of the PL signals with increasing Ge deposition are correlated with the three-dimensional growth. However, for an unambiguous clarification some more experimental data may be useful, such as the measurement of the luminescence spectra at the onset of island formation. This may help to distinct between the PL originating from the wetting layer and the Ge dots.

ACKNOLEDGEMENTS

The authors like to acknowledge the support of their collegues at PSI, Hans Sigg and Heinz Siegwart for their help on PL measurements, Theresa Mezzacasa and Dieter Bächle for their support in clean room processing steps. They are indebted to Klaus Kern (EPFL) and Klaus Ensslin (ETHZ) for their input. Without their work, their ideas and valuable discussions, this work would not have been possible. Part of the studies presented in this paper was supported by the swiss national foundation, contract numbers 2129-45434.95 and 2100-045512.95/1.

REFERENCES

1. Terashima, M. Tajima, and T. Tatsumi, *Appl. Phys. Lett.* **57**, 1925 (1990)
2. J.C. Sturm, H. Manoharan, L.C. Lenchyshyn, M.L.W. Thewalt, N.L. Rowell, J.P. Noël, and D.C. Houghton, *Phys. Rev. Lett.* **66**, 1362 (1991)
3. U. Gnutzmann and K. Clausecker, *Appl. Phys.* 3, 9 (1974)
4. E. Kasper, H. Kibbel, H. Jorke, H. Brugger, E. Friess, and G. Abstreiter, *Phys. Rev.* B **38**, 3599 (1988)
5. B. Delley and E.F. Steigmeier, *Phys. Rev.* B **47**, 1397 (1993)
6. L.T. Canham, *Appl. Phys. Lett.* **57**, 1046 (1990)
7. M.S. Brandt, H.D. Fuchs, M. Stutzmann, J. Weber, and M. Cardona, *Solid State Commun.* **81**, 307 (1992)
8. S.M. Prokes, O.J. Glembocki, V.M. Bermudez, R. Kaplan, L.E. Friedersdorf, and P.C. Searson, *Phys. Rev.* B **45**, 13788 (1992)
9. Y.H. Xie, W.L. Wilson, F.M. Ross, J.A. Mucha, E.A. Fitzgerald, J.M. Macaulay, and T.D. Harris, *J. Appl. Phys.* **71**, 2403 (1992)
10. F. Koch, *Microelectronic Engineering* **28**, 237 (1995)
11. L. Canham, *Phys. World*, **41** (1992)
12. C. Zibyll and V. Petrova-Koch, *Angew. Chem.* **105**, 887 (1993)
13. Y.-W. Mo, D.E. Savage, B.S. Swartzentruber, and M.G. Lagally, *Phys. Rev. Lett.* **65**, 1020, (1990)
14. D.-J. Eaglesham and M. Cerullo, *Phys. Rev. Lett.* **64**, 1943 (1990)
15. B. Voigtländer and A. Zinner, *Appl. Phys. Lett.* **63**, 3055 (1993)
16. J. Tersoff, C. Teichert, and M. Lagally, *Phys. Rev. Lett.* **76**, 1675 (1996)
17. R. Apetz, L. Vescan, A. Hartmann, R. Loo, C. Dieker, R. Carius, and H. Lüth, *Mater. Sci. Technol.* **11**, 425 (1995)
18. P. Schittenhelm, C. Engel, F. Findeis, G. Abstreiter, A.A. Darhuber, G. Bauer, A.O. Kosogov, and P. Werner *J. Vac. Sci. Technol.* B **16**, 1575 (1998)
19. S.S. Iyer, K. Eberl, M.S. Goorsky, F.K. LeGoues, J.C. Tsang, F. Cardone, *Appl. Phys. Lett.* **60**, 356 (1992)
20. K. Eberl, S.S. Iyer, and F.K. LeGoues, *Appl. Phys. Lett.* **64**, 739 (1994)
21. K. Brunner, K. Eberl, and W. Winter, *Phys. Rev. Lett.* **76**, 303 (1996)
22. W.-X. Ni, A. Henry, M.I. Larsson, K. Joelsson, and G.V. Hansson, *Appl. Phys. Lett.* **65**, 1772 (1994)
23. M.L.W. Thewalt, D.A. Harrison, C.F. Reinhard, J.A. Wolk, and H. Lafontaine, *Phys. Rev. Lett.* **79**, 269 (1997)
24. B.L. Stein, E.T. Yu, E.T. Croke, A.T. Hunter, T. Laursen, A.E. Bair, J.W. Mayer, and C.C. Ahn, *Appl. Phys. Lett.* **70**, 3413 (1997)
25. R. Hartmann, U. Gennser, , H. Sigg, D. Grützmacher and K. Ennslin *Appl. Phys. Lett.* **73**, 1257 (1998)
26. S. Ando; T. Honda; N. Kobayashi, Jap. *J. of Appl. Phys. Part 2 (Letters)* **32**,; L104-6. (1993)
27. E.A. Fitzgerald, G.P. Watson, R.E. Proano, D.G. Ast, P.D. Kirchner, G.D. Petit, and J.M. Woodhall, *J. Appl. Phys.* **65**, 2220 (1990)
28. G. Abstreiter, P. Schittenhelm, C. Engel, E. Silveira, A. Zrenner, D. Mertens, and W. Jäger, *Semicond. Sci. Technol.* **11**, 1521 (1996)
29. K. Eberl; O.G. Schmidt; S. Schieker; N.Y. Jin-Phillipp; F. Phillipp, *Solid-State-Electronics*.**42**, 1593 (1998)
30. O. Leifeld, D. Grützmacher, K. Kern, E. Kaxiras, and P. Kelires, *Phys. Rev. Lett.* Januar (1999)
31. O. Leifeld, B. Müller, D. Grützmacher, and K. Kern, *Appl. Phys. Lett* (accepted)
32. N. Usami, Y. Shiraki, and S. Fukatsu, *Appl. Phys. Lett.* **68** 2340 (1996)
33. S. Fukatsu, H. Sunamura, Y. Shiraki, and S. Komiyama, *Appl. Phys. Lett.* **71**, 258 (1997)
34. H.J. Osten, M. Kim, K. Pressel, and P. Zaumseil, *J. Appl. Phys.* **80**, 6711 (1996)
35. K.B. Joelsson, W.-X. Ni, G. Pozina, H.H. Radamson, and G.V. Hansson, *Appl. Phys. Lett.* **71**, 653 (1997)
36. S. Schieker, O.G. Schmidt, K. Eberl, N.Y. Jin-Phillipp, and F. Phillipp, *Appl. Phys. Lett.* **72** 3344 (1998)